Received: 5 May 2023 | Revised: 3 July 2023 | Accepted: 12 July 2023

DOI: 10.1002/appl.202300044

RESEARCH ARTICLE

Applied Research

The photon-electrical conversion efficiency of dye-sensitive solar cells fabricated using a highly conductive silver-nanoparticle/titania photocathode

Likius S. Daniel[1,2] | **Rocha T. Kaffer**[1] | **Loini M. Kalipi**[1] | **Ateeq Rahman**[1] | **Mbela Kalengay**[1] | **Veikko Uahengo**[1]

[1]Department of Physics, Chemistry and Material Science, University of Namibia, Windhoek, Namibia

[2]Multidisciplinary Research Service, Centre for Research Services, University of Namibia, Windhoek, Namibia

Correspondence
Likius S. Daniel and Ateeq Rahman, Department of Physics, Chemistry and Material Science, Postbag 13301, University of Namibia, Windhoek, Namibia.
Email: daniels@unam.na and arahman@unam.na

Funding information
National Commission on Research, Science and Technology

Abstract

The TiO_2 thin film, Ag NP and three Ag-NP/TiO_2 composite thin films (COMP-Ag_n; n = 20, 50, and 75 Ag mol%) were successfully fabricated on quartz glass. The optical properties of the composite electrodes were investigated, and the results indicate a surface plasmonic resonance peak at 410 nm while the electrical resistivity of the composite thin films improved up to 6.9×10^{-5} Ω cm. The photo-response threshold of the Ag-NP/TiO_2 composite thin films was enhanced and shifted into the visible and near-infrared when the chlorophyll dye was adsorbed onto them. The hall effect was performed on the fabricated thin films and the charge carrier concentrate value confirmed that the Ag/TiO_2 with Ag concentrate >45% are found to be p-type. The n-types were observed till the Ag content in TiO_2 was increased up to 45 mol%. COMP-Ag75 has a charge carrier concentration of 1.3×10^{-19} cm^{-3} as a p-type electrode was then employed to construct a p-DSSC. Such enhancement on photovoltaic activity can be attributed to the generated Z-scheme system in the anatase/rutile phase-junction Ag/TiO_2 photocathode enhances the separation, diffusion, and transformation of electron/hole pairs inside the structure. This p-DSSC exhibits a photon-electrical conversion efficiency (PCE) of 0.37%. The PCE recorded is equal to or greater than those of traditional high-efficiency n-DSSCs. This allows the creation of a new generation of photocathodic p-DSSCs with previously unheard-of unprecedentedly high concentrations of Ag (up to 80 mol%) evenly scattered in a TiO_2 matrix, and this efficacy is the highest ever reported for a p-type working Ag/TiO_2/chlorophyll/iodine electrode. This may enable the use of this electrode as a component of photosensitizer tandem devices.

KEYWORDS
molecular precursor method, p-DSSC, photocathode, plasmonic, p-type, silver, titania

INTRODUCTION

Photovoltaic (PV) cells termed as dye-sensitized solar cells (DSSCs) convert light energy directly into electrical energy with an assistance of dye. In recognition of their creator, Michael Gratzel, they are sometimes referred to as Gratzel cells [1]. In-depth research has been accomplished on p-DSSC's capacity to transform solar energy [2-4]. The number of metal oxides that exhibit p-type conductivity is smaller than that of n-DSSCs, for which photoanodes made of various semiconductors, such as TiO_2, ZnO, and Nb_2O_5, have been exploited [1, 5, 6]. The photocathode of p-type DSSCs is made of a nanostructured p-type semiconductor (NiO, K/ZnO, $CuFeO_2$) that has been dye-sensitized to effectively absorb solar radiation [7-10]. He et al. [8] reported the first p-DSSC in 1999 using nickel oxide film as photocathodes for solar cells. Having a wide bandgap (E_g) of 3.6–4 eV and being intrinsically nonstoichiometric, nickel oxide is a p-type semiconductor that is both thermally and chemically stable. The cell was developed employing identical components as an n-DSSC, however, instead of TiO_2 semiconductor, a thin film of p-type NiO semiconductor was utilized. Erythrosin B was employed as a sensitizer to produce a photon-electrical conversion efficiency (PCE) overall of 0.0076% [8]. p-DSSCs have lately attracted considerable interest because of the possibility of employing them as parts of photosensitizer tandem devices (p-n-DSSCs) [4]. Although the operation of p-type devices is identical to that of n-type DSSCs, the flow of electrons occurs in the opposite direction because the majority of charge carriers in metal oxides are positive holes (h^+) [11]. In p-DSSC, electrons move from the semiconductor valence band to the sensitizer. The oxized redox mediator helps transfer electrons from the reduced dye molecules to the counter electroode (CE). [11] The electrons then join the same device at the working electrode after going through the external circuit.

The p-DSSC's overall structure is made up of four key components. The working electrode is the first major component. The TCO glass substrate is coated with a thin film of a semiconductor, typically p-type NiO [8]. The sensitizer introduces holes into the p-type semiconductor's valence band upon photoexcitation [12]. In this research, a conductive, semi-transparent p-type Ag/TiO_2 thin film fabricated on quartz glass is introduced to replace conventional TCO electrode act as a working electrode in DSSCs. Numerous studies have been conducted on titanium dioxide by doping it with various chemicals to modify its threshold energy to function with visible light [13–15]. In specific surface plasmon-enhanced cells, the dye that is adsorbed on silver nanoparticles (NPs) absorbs light with greater efficiency [16, 17]. The localized surface plasmon resonance (LSPR) principle is employed in several solar cell topologies to increase photo-responsive and photoelectrochemical reactions [18, 19]. The maximum efficiency of the n-DSSCs surface plasmon-enhanced devices was 10.2% [20]. Daniel et al. [21–23] showed that molecular precursor method (MPM) can be utilized to fabricate Ag/TiO_2 composite thin films on quartz glass with different and unprecedentedly high concentrations of Ag (up to 80 mol%) evenly dispersed in a TiO_2 matrix. A blended precursor solutions made of a Ti complex of EDTA solution and a silver complex of dibutyl amine was used to generate exceptional Ag/TiO_2 thin films [20, 21]. Ag/TiO_2 composite thin film fabricated by MPM are "intrinsic nonstoichiometric" photocathode electrodes with wide bandgap (E_g 3.6–4 eV), exhibiting good electrical conductivity and chemical stability. During UV and visible (vis) light irradiation, the cathodic photocurrent densities produced by Ag/TiO_2 composite thin film with Ag concentrations more than 0.45 mol ratio were observed [23]. This was concluded that the Ag-TiO_2 thin films fabricated are p-type while pure TiO_2 fabricated with the same method was n-type as they gave a cathodic and an anodic photocurrent, respectively. Moreover, the Ag/TiO_2 composite with the Ag component, of 0.50 molar ratio recorded the lowest electrical resistivity of 10^{-5} cm at 25°C [21]. In addition, even though they can function as a photocatalyst when exposed to UV radiation, composite thin films of Ag that contain less than 40 Ag mol % are ineffective when exposed to visible light [21]. Their thickness ranged from 100 to 260 nm. However, composite thin film that contain more than 40% Ag mol% in titania do respond to visible light due to Ag surface plasmonic resonance effect. These parameters were used to fabricate Ag-NP/TiO_2 composite thin films with a variety of Ag volumetric percent values up to 75% mol of Ag in titania using MPM to examine PCE of p-type dye-sensitive solar cells.

The sensitization dye is the second component. As sensitizers in DSSCs, synthetic dyes, and organic plant-based dyes are usually employed to increase the discharge of short-circuit current density (J_{sc}) in visible range. The most studied sensitizer dye is ruthenium based, a synthetic dye. The N3, N719, and "black" dyes created by the Grätzel group are said to be the most effective dye sensitizers proven to date [24]. In fact, ruthenium compounds are effective sensitizers in n-DSSCs and have long outperformed organic dyes [25]. Contrary to the majority of n-DSSCs, dyes based on ruthenium complexes typically perform poorer than organic dyes in p-DSSCs. Alhamed et al. [26] research supports earlier studies' findings that natural dyes perform better in PV applications than the Ru dye N_3 utilized in Grätzel cells. For their cells, they recorded a 0.04% for chlorophyll and 3.04% efficiency by combing the natural dyes. Natural dyes are currently receiving more attention in the context of green chemistry due to their abundance, low cost of metal complex sensitizers, ease of extraction, safety—they pose no threat to the environment, are nontoxic, can replace costly chemical synthesis processes through straightforward extraction processes, and are fully biodegradable [27]. Natural dye sensitizers come in a variety of forms; to name a few, anthocyanin, carotenoid, flavonoid, and chlorophyll pigments are taken from the petals, roots, leaves, fruits, and plants of flowers [28]. It was revealed that chlorophyll was more effective than the other pigments [29]. Unfortunately, stability issues lead to decreased effectiveness [30]. Xanthophylls have demonstrated improved stability and greater absorption [31]. Pigments that can absorb photons are not present in all vegetative organs. The leaves are the primary component of the plant from which chlorophyll is extracted for use in DSSC [27]. However, another study has revealed that plant stems have increased efficiency of about 0.740% [32]. This dispels the common misconception that the

only component that performs well is the leaf. Never the rest, one cannot simply choose whatever plants they please; a correct line of reasoning must be adhered to. Chlorophyll can be easily acquired from plant materials, and because it is environmentally beneficial and biodegradable, it was taken into consideration for this study. It was therefore reasonable to select chlorophyll. In this research, chlorophyll as a dye sensitizer was extracted from plant leaves and due to the abundance of *Colophospermum mopane* trees, the Mopane tree leaves were used for the extraction of chlorophyll.

The electrolyte, which can be either solid electrolytes or organic or inorganic solvents, is the third component of a DSSC. Redox coupling in an electrolyte can be between the species I^-/I^{-3}, Br-/Br^{-2}, SCN^-/SCN_2, and Co (II)/Co (III) [33]. Cobalt (II/III) complexes in particular have found use in p-DSSCs as electrolytes, providing open-circuit potentials (V_{oc}) of up to 350 mV [34]. These complexes, however, have not led to an overall improvement in the efficiency of energy conversion of p-DSSCs above the 0.5% threshold [35]. Perela and his group [36] reported the use of tris(acetylacetonato)iron (III)/(II) Redox Couple ($[Fe(acac)^3]^{o/1-}$) for p-DSSCs using NiO as a CE. It was discovered that this cell had the highest reported short circuit current (J_{SC} = 7.65 $mAcm^{-2}$), and energy conversion efficiency (2.51%) with a fill factor (FF) of 0.51 and an open-circuit voltage V_{OC} = 645 mV [36]. The most popular redox coupling, I^-/I^{-3} has been employed in all most in p-DSSCs studied [33]. However, this redox coupling is highly volatile, corrodes the glass substrate, metal oxides, and Pt, and causes the decomposition of the dye with diminished stability over time. Even though there are numerous possible alternatives to this redox coupling such as the use of solid-state based electrolytes, [37] they are severely constrained when compared to $I^{-/}I^{-3}$ coupling. When compared to previously published figures, the use of this redox pair increased photocathode efficiency by more than a factor of two (1.3%) and V_{OC} by a factor of two (709 mV) [9, 38–40]. In this research, $^-I/I^3$ was employed as redox mediators.

The CE, employed to speed up the reduction process of electrolytes, is the final component. A catalyst like platinum (Pt) is typically applied to glass substrates, acting as a CE. The redox couple affects the CE activities that are used to transfer photogenerated charges across the working and CEs. CE initiates the reduction of electrolyte species, which gathers the holes from the hole transport materials (HTMs) [41]. The CE's ability to accept electrons from the external circuit and minimize the redox species that aid sensitizer regeneration following electron injection affects solar cell PCE, durability, and affordability [41]. The scientific community has recently paid a great deal of attention to dye CE-based DSSC technologies to maximize incident light harvesting and performance [6]. To enable improved light harvesting, the CE can be coated with mesoporous activated carbon (AC) or carbon nanotube (CNT) [42]. AC is used in DSSC as a sensitized dye adsorbent and as a conductor. This is because, in addition to being a green economy, the prepared AC's characteristics can provide a lot of active sites for dye molecules to adhere to, creating an electron channel for the electrochemical processes [43]. This interaction is thought to increase the effectiveness of the p-DSSC [44]. FF is recommended as one of the PV characteristics that impacts the efficiency of DSSCs in AC-based solar cells [45]. Higher FF and high PCE were said to be produced using hybrid AC cells [46]. Traditionally, to enhance the overall conductivity of the CE, the transparent conductive oxide (TCO) glass substrate such as fluorine-doped tin oxide (FTO) or indium-doped tin oxide (ITO) is used as a supportive media for the AC layer [47]. The transparency of TCO glass should be greater than 80%, and they should also have a higher charge transfer rate. As a result, conductivity is improved, and energy losses are decreased. Conventional DSSC rely on FTO or ITO electrodes that include pricey rare elements, which are challenging to fabricate. The glass substrate can be selected based on the experiment and the resources that are available. The optical transmission of FTO is high (at least 90%) and unaffected by fluorine doping in the visible region [48]. There is also no indium present to potentially diffuse into the electrolyte, FTO is less costly to fabricate and the susceptibility to surface cleaning techniques is diminished than ITO [49, 50]. There are also newly fabricated TCO materials such as magnesium tin oxide (MTO) and aluminum doped zinc oxide (AlZnO), [51, 52] with potential to be used in PV applications. The CE in this study was prepared by coating FTO with mesoporous AC paster to create an active site for the cell.

The n-DSSCs have been claimed to have energy conversion efficiencies as high as 13%, [53] while p-DSSCs have only achieved 2.51% [36]. In p-DSSCs, this disparity is mostly brought about by problems with the electrolytes employed thus far and the photocathode electrode [38]. Using the most effective p-DSSC sensitizer available, a porous NiO nanoparticles layer, and an I^-/I^{-3} based electrolyte, photocathodes were able to attain PCE of up to 0.41% under sunlight irradiation of 1000 W m^2, AM 1.5 G [36]. The NiO-sensitized photocathode displays short-circuit current densities (J_{SC}) of up to 5.35 mA cm^2 and open-circuit voltages (V_{OC}) of up to 218 mV [4]. Despite this significant development, p-DSCs still lag their n-type counterparts in performance. Lower open-circuit potentials are one of these p-DSCs' main performance constraints. Its V_{OC} is influenced by the difference between the electrolyte's redox potential and the p-type semiconductor's quasi-Fermi level. Recent developments for p-type DSSCs include the use of different nanocrystalline metal oxides to be more specific, NiO (218 mV), $CuAlO_2$ (V_{OC} = 333 mV), and $CuGaO_2$ (V_{OC} = 357 mV) coated on TCO substrates were studied [36, 54]. This article presents the fabrication of a highly conductive p-type Ag/TiO_2 coated on a naked glass instead on conventional TCO, the assembling of its p-type DSSC and its PV parameters are presented. This is the first time a highly conductive silver nanoparticle/titania photocathode-based DSSC is reported.

The titania-based electrode of the sensitized solar cell always performs better because of the plasmonic impact of noble elements like Ag or Au when they are introduced [16, 20, 55]. Different plasmonic materials of different Ag molar concentration in TiO_2 will result in various effects [56, 57]. Here, we show how unprecedentedly high concentrations of Ag nanoparticles in a mixture of anatase and rutile matrix affects a DSSC's electron flowing direction. We introduce a p-type architecture for organic solar cells where the active region is sandwiched between Ag/TiO_2 thin film and AC-FTO

film. Ag/TiO_2 thin film was fabricated by MPM. MPM can be utilized to fabricate Ag/TiO_2 composite thin films on quartz glass with different and unprecedentedly high concentrations of Ag (up to 80 mol%) evenly dispersed in a TiO_2 matrix [21–23]. The hall effect was performed on the fabricated thin films in this paper and the charge carrier concentrate value confirmed that the Ag/TiO_2 with Ag concentrate >40% are found to be p-type. The 75% Ag/:25%TiO_2 p-type electrode was then employed to construct a p-DSSC. The term p-DSSC means here, a layer sequence in the form Ag/Titania photocathode electrode layer, intrinsic layer, and AC-FTO layer. A *FF* value of 0.335 and a PCE of 0.37% were displayed by the newly created nanostructured Ag/Titania p-DSSC. To our knowledge, this is the first p-DSSC with previously unheard-of high quantities of Ag (75 mol%) evenly scattered in a TiO_2 matrix, and this efficiency is the highest performance achieved among the Ag/TiO_2/Chlorophyll/Iodine adopting p-type working electrode reported so far.

MATERIALS AND METHODS

Chemical used

Silver acetate, Na_2SO_4, dibutylamine, ethanol, H_2O_2 (30% pure), ethylenediamine-N,N,N',N'-tetraacetic acid (EDTA) and titanium tetra-isopropoxide ($Ti(O_iPr)_4$) were purchased from GenMed cc Chemical Co., Inc, and were used without further purification. Glasses ($20 \times 20 \times 1.5\ mm^3$) were order from PG Glass Co., Ltd. These glass substrates were prepared and cleaned with 2-propanol in an ultrasonic bath to remove physiosorbed organic molecules from the surfaces. This was followed by rinsing several times with de-ionized water. The substrates were then dried in a drying oven at 70°C.

Preparation of coating solutions and fabrication of COMP-Agn

As per MPM, a precursor solution containing a Ti^{4+} compound of EDTA, S_{TiO2}, was prepared, as reported by Sato and his team [21, 58–60]. A silver acetate-ethanol solution, S_{Ag}, was prepared using a technique we recently disclosed, [21–23] to fabricate AgNPs for exploitation in composite thin films. Using the S_{TiO2} and S_{Ag} precursor solutions, respective thin films of TiO_2 and Ag NP were fabricated on quartz glass substrates at 600°C in air. The coating solutions for COMP-Ag*n* were prepared by combining the S_{TiO2} and S_{Ag} solutions at Ag molar concentrations (*n*), where *n* = 0, 20, 50, 75, and 100 mol%, respectively. Three COMP-Ag*n* films were fabricated on $4 \times 2\ cm^2$ quartz glass substrates at 600 C in the air. Pure TiO_2 thin film and Ag-NP were also coated on a glass substrate. Table 1 lists the film thickness, electrical resistance, and electrical resistance, averaged photocurrent density (APD) under vis- and UV-light and averaged dark current density (ADD) of the COMP-Ag*n* films adapted from the previous studies [21, 23].

Photoelectrode characterization

The XRD, SEM, XPS, optical properties, photocurrent density, and electrical conductivity results of TiO_2 thin film, Ag NP, and three Ag-NP/TiO_2 composite thin films (COMP-Agn; *n* = 20, 50, and 75 Ag mol%) fabricated are presented in our previous papers [21–23]. Photoluminescence (PL) spectra for pure TiO_2 and COMP-Ag-75 was acquired by using the 340 nm line of a nanosecond Nd:YAG laser (NL303G) as excitation source at room temperature via PerkinElmer LS-55.

Electrical analysis using Hall effect measurement

DC-Hall effect measurements were carried out using Swin system. The measurements setup for this instrument employs four probes method. The COMP-Ag20-75 samples that were coated onto quartz glass substrates underwent electrical testing, separately. Under dark conditions and at room temperature, the electrical resistance (Ω), resistivity (Ω cm), charge carrier concentration (n/cm^{-3}), and carrier mobility ($cm^2V^{-1}s^{-1}$) were measured. On a surface of 2 by 2 cm^2, measurements were performed using a current of 1 mA and a

TABLE 1 Film thickness, electrical resistance, averaged photocurrent density (APD) under vis- and UV-light, and averaged dark current density (ADD) of the TiO_2, Ag NP, and COMP-Ag*n* films fabricated at 600°C on the quartz glass substrates, where *n* = 20, 50, and 75 Ag mol%.

Notation (*n*)	Film thickness (nm) [21]	Electrical resistance[a] (Ω) [21]	APD,[ab] Vis-light UV-light (μA/cm^2) [23]	ADD,[ab] Dark (μA/cm^2) [23]	Photocurrent polarity [23]
Pure TiO_2	130	$>10^8$	ND 1.0 (3)	ND	Anodic
COMP-Ag20	150	$>10^8$	ND ND	ND	—
COMP-Ag50	100	5.0 (0.1)	−10 (1) −1 (1)	−2 (1)	Cathodic
COMP-Ag75	110	7.0 (3)	−10 (2) −1.2 (3)	−2.8 (4)	Cathodic
pure Ag NP	Rough	$>10^8$	—	—	—

[a]The standard deviations are presented in parentheses.

[b]ND; Current generated is smaller than 10 nA.

permanent magnet of 0.53 T. The sheet resistance (Rs) was calculated using the below equation:

$$\text{Sheet resistance } (Rs = \Omega/\blacksquare) = \frac{\text{Bulk resistivity } (\rho = \Omega\text{cm})}{\text{Film thickness } (t = \text{nm})}. \quad (1)$$

Extraction of chlorophyll as dye sensitizers from *C. mopane* dry leaves

In the Omusati region of northern Namibia, dry leaves were collected from the Mopane tree, scientifically known as *C. mopane* and known locally as Omusati. Omusati area, in Northern Namibia, gets its name from the number of mopane trees that can be found there. Two hundred milliliters of 95% methanol were used to dissolve 20 g of dry leaf powder [61, 62]. The sample was kept in the cabinet for a week. After then, the sample was filtered. The samples of filtrate were then immediately taken to the lab for examination and coating. Utilizing the double-beam mode, chlorophyll absorption spectrum was measured from 200 to 800 nm using a Hitachi U-2800 spectrophotometer and 95% methanol as a reference. The photometric of chlorophyll-*a* and -*b* in the samples were determined. Chlorophyll contents found in the cell extract are spectrophotometrically estimated by measuring absorbance at 664, 615, and 538 nm. Modified formulae by Lichtenthaler and Buschmann, [63] and Johan et al., [64] were used to measure the chlorophyll concentration value. Refer to the below equations.

$$\text{Chl-}a\left(\frac{\mu g}{L}\right) = (11.\,85 \times E_{664}) - (1.\,54 \times E_{615} - (0.\,08 \times E_{538}), \quad (2)$$

$$\text{ConcentrationofChl} - a\left(\frac{mg}{L}\right) = \frac{[\text{Chl} - a \times v]}{V{\cdot}L}, \quad (3)$$

where, *v*, volume of acetone 90%, *V*, Volume of water sample, *L*, light path of cuvette, E_{664} = value of absorbance at wavelength 664 nm, E_{615} = Value of absorbance at wavelength 615 nm and E_{630} = value of absorbance at wavelength 630 nm.

The concentration of the extracted chlorophyl-*a* and -*b* obtained were 0.53 and 0.42 mg/L, respectively. The concentration of chlorophyll-*a* is higher than of chlorophyll-*b* as expected and reported in literature [63]. Figure 1a,b shows the photographs of Mopane plant leaves and Chlorophyll extracted in methanol solvent. FTIR technique was used to analyze the functional groups of the extracted chlorophyll dye. The spectrum was recorded in the range of 4000–400 cm^{-1} using Opus software (version 6.5.6) on Bruker Platinum Tensor 27 ATR-IR Spectrophotometer.

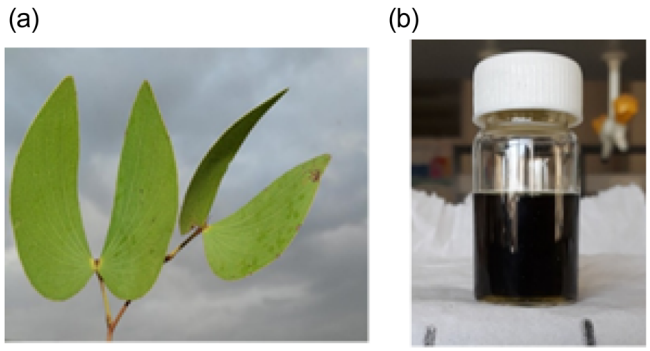

FIGURE 1 (a) Mopane plant leave, (b) chlorophyll dye extracted in methanol solvent.

Fabrication of COMP-Agn photocathode/chlorophyll dye sensitizer work electrode

All five of the prepared thin films were deep-coated for 48 h with a solution of prepared chlorophyll dye sensitizer with a mixed concentration of chlorophyll-*a* at 0.53 mg/L and of chlorophyll-*a* at 0.42 mg/L, respectively. The excess sensitized dyes were then removed by soaking them in ethanol for 5–10 s, followed by two days of drying at 100°C to produce TiO_2-Chl, AgNP-Chl, COMP-Ag_n/Chl dye sensitized thin films. Utilizing the double-beam mode, the absorption spectra for these thin films created on quartz glass substrates were measured. Figure 2 shows the photographs of fabricated TiO_2-Chl, Ag NP-Chl, COMP-Agn/Chl dye sensitized thin films, respectively. TiO_2, Ag NP-Chl, COMP-Ag25/Chl, and COMP-Ag50/Chl do not allow more dye molecules to be adsorbed, thereby obviously not improving the light-harvesting efficiency. According to

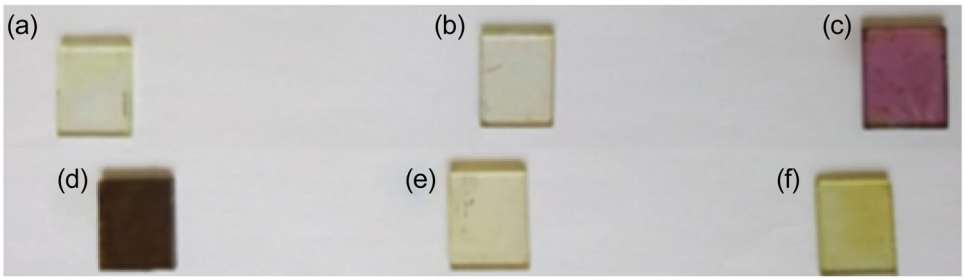

FIGURE 2 Photographs of (a) pure TiO_2-Chl, (b) COMP-Ag25/Chl, (c) COMP-Ag50/Chl, (d) COMP-Ag75/Chl, (e) Ag NP-Ch, and (f) Chl dye sensitized thin films on quartz glass, respectively.

the SEM image already reported for these thin films, there aren't many Ag particles at the lower Ag load (Ag < 40 mol%), and a few of those present are scattered widely across the film surface [21]. Although this resulted in partial agglomeration as the silver load increased, for silver loading when Ag > 40 mol%, many porous Ag particles are uniformly dispersed over the films [21]. Thus COMP-Ag75 has absorbed chlorophyll dye better compared to other thin films, and it became even darker. Ag nanoparticle aggregation in this thin film results in morphological changes that increased film thickness and create porous on the surface, which is necessary for adsorption. Hence, COMP-Ag75 was the only one used as a photocathode electrode for the preparation of p-DSSC in this research.

Fabrication of FTO/AC CE

The AC prepared following authors' published procedure by Ateeq et al. [65] with Brunauer–Emmett–Teller surface area in the range 121–372 m^2/g, pore volumes between 0.0239 and 0.0483 cm^3/g and pore diameters between 21 and 45 Å was used. This is because, in addition to being readily available, the prepared AC's characteristics can offer a lot of surface area for molecules to adhere to, creating an electron channel for the creation of an active catalytic sites for charge storage and electrochemical processes [66]. To prepare AC paste, 5.00 g of AC was mixed with drops of ethanol, ethylene glycol, and water to form an even paste. A doctor blade method was used to apply the AC paste on FTO (FTO/glass, 8 $\Omega\blacksquare^{-1}$, 2.3 mm-thick, Pilkington TEC8) substrates to produce a CE. Figure 3 shows the photograph of the prepared FTO/AC as a CE.

Preparation of p-DSSC device and evaluation of their performances

For the fabrication of the p-type DSSC, COMP-Ag75 was selected from the fabricated composites since it adsorbs chlorophyll better as shown above, had high electrical conductivity [21] and generated the highest photocathodic in the visible light region [23]. The COMP-Ag75/Chl prepared photocathode, henceforth referred to as Ag/TiO_2 plasmonic conductive nanocomposite photocathode, was submerged in a methanolic solution of mixed concentration of chlorophyll-*a* at 0.53 mg/L and of chlorophyll-*a* at 0.42 mg/L for 24 h at room temperature under dim lighting. After being removed from the solution, the dye-adsorbed plasmonic photocathode was quickly but carefully cleaned with methanol. A dye-absorbed photocathode was placed on top of a prepared FTO/AC CE, and they were tightly clamped together. 20 ml of ethylene glycol was used to dissolve 0.25 g of iodide crystals. After that, 0.82 g of potassium iodide was added, and the mixture was agitated to produce a triiodide electrolyte. Through capillary action, a triiodide electrolyte standard solution was added to the p-DSSC. The performance of the p-DSSC was assessed using an active area of 2.25 cm^2. An Avaspec-2048 fiber optic spectrophotometer was used to quantify the sunlight

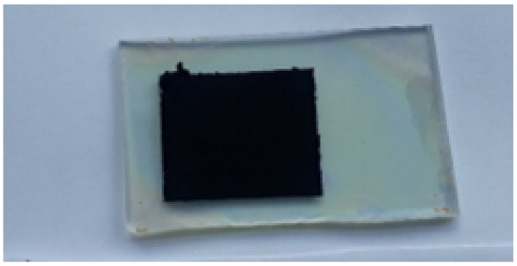

FIGURE 3 The prepared fluorine-doped tin oxide/activated carbon counter electrode.

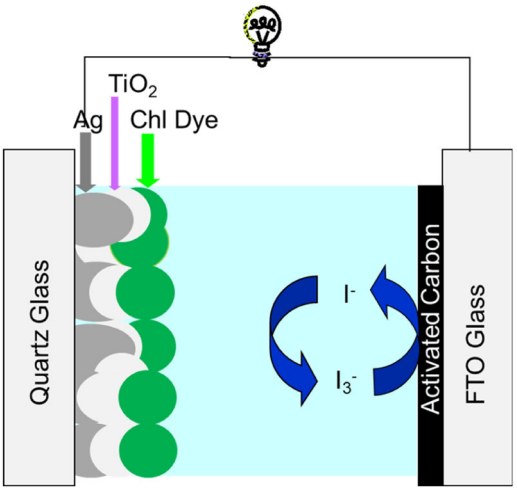

FIGURE 4 Schematic of a p-type architecture for dye-sensitized solar cells where the active region is sandwiched between Ag/TiO_2/Chl thin film and activated carbon-fluorine-doped tin oxide film.

intensity before measuring the PV parameter. The following test conditions were used: A cloudless sky, 0.58 mW/cm^2 solar radiation and 30°C outside temperature. When measurements were made, the device was positioned with its back to the sun at a 45° angle. Using a computer-controlled Potentiostat 466, the photocurrent signal measurement (J-V curve) properties of the p-DSSCs were examined. The cell was tested with a power input of 780 mW while exposed to direct sunshine. The results were then checked for consistency over at least four runs of the analysis. Using Echem software, the machine automatically generated a J-V curve for the constructed cell. Figure 4 shows a p-type architecture for organic solar cells where the active region is sandwiched between Ag/TiO_2 thin film and AC-FTO film.

RESULTS AND DISCUSSION

The TiO_2 thin film, Ag NP, and three Ag-NP/TiO_2 composite thin films (COMP-Agn; n = 20, 50, and 75 Ag mol%) were fabricated on quartz glass. The XRD, SEM, XPS, optical properties, photocurrent density, and electrical conductivity results of these thin films are presented in our previous papers [21–23].

Hall effect measurements

Using a four-probe DC-Hall effect assessing approach, the electrical characteristics of the developed Ag-doped TiO_2 thin films were investigated. The results are presented in Table 2, which disclose that the electrical resistivity (R) registered for the Ag/TiO_2 composite thin films with Ag mol% <50 was higher ($R \times 10^4 \Omega$) when compared to the Ag-doped TiO_2 thin films with Ag mol% ≥50% ($R \times 10° \Omega$).

The bulk resistivity (R_s) measured trend for 300 K was determined to be declining from 45% to 75% Ag-doped TiO_2 thin films (from $\rho \times 10^1\ \Omega$ cm to $\rho \times 10^{-5}\ \Omega$ cm). Moreover, the sheet resistance calculated showed a decreasing trend as the Ag mol% is increasing in glass-coated TiO_2 thin films (from $R_s \times 10^4\ \Omega/\blacksquare$ to $R_s \times 10^0\ \Omega/\blacksquare$), corresponding to a semiconductor (COMP-Ag20 to Ag40 thin films) and to a corresponding to a metal (COMP-Ag50 to Ag70 thin films), respectively. Increasing the doping level to 75% enhances conductivity and the charge carrier concentration. This agrees with the previous finding [21].

The bulk of carriers displayed high mobilities, which is essential for semiconductor functionality, as carrier mobility also showed a rising trend [67]. In terms of the doping of the films, Table 2 shows that the concentration of carriers clearly increased, but the mobility values at room temperature decreased with an increase in the doping ratios. The COMP-Ag20 and Ag40 displayed an n-type conductivity as electrons are the prominent (minority) type of carrier concentrations (N) in the range of $^{-}N \times 10^{14}$ to $^{-}N \times 10^{12}\ cm^{-3}$, respectively. COMP-Ag70 has the lowers sheet resistance to $6.27\ \Omega\blacksquare^{-1}$, with the highest major charge carrier concentration of $1.3 \times 10^{19}\ cm^{-3}$ but the lowest charge carrier mobility ($780\ cm^3\ V^{-1}\ s^{-1}$). These measurements showed that the fabricated thin films with Ag mol% less than or equal to 45 are of the negative type (n-type), through the negative sign of the concentration of the minority carriers. Meaning they are anodic electrodes. Moreover, the prepared thin films with Ag mol% greater than 45 are of the positive type (p-type), through the positive sign of the concentration of the majority carriers. These results agree with other researchers, [23] whereby the same thin films gave an anodic and cathodic photocurrent, respectively. Also, the COMP-Agn high's electrical conductivity reported [22] and charge carrier observed during Hall effect measurement is crucial for enabling a photo responsive activity by boosting the better precision of charge carrier separation. The electrical bulk resistivity of the COMPAg75 is $10^{-5}\ \Omega$ cm.

Absorption spectra of TiO_2, Ag-NP, and COMP-Agn thin films

The absorption spectra of thin films fabricated of TiO_2, Ag-NP, and COMP-Agn (n = 20, 50, and 75 Ag mol%) are shown in Figure 5 below. UV-vis spectroscopy was used to examine thin films. Due to its broad band gap, which is restricted to the UV-light, the pure TiO_2 thin film did not exhibit any absorbance peak in the visible range. A value of 3.61 eV was obtained by extrapolating the optical band gap of the TiO_2 thin film, [23] which is equivalent to the band gap of pure anatase (assuming direct transition) [68]. According to our earlier research, all COMP-Agn films had band edges that were identical to those of pure TiO_2 thin films, [23] hence the incorporation of Ag NPs into the TiO_2 matrix had no impact on the band gap of TiO_2.

The presence of silver nanoparticles was confirmed by the Ag NP thin film's visible absorbance peak, which peaked at 410 nm and surface plasmon resonance (SPR) is the cause of this observation [15]. The local electromagnetic fields surrounding the nanoparticles are strongly enhanced because of the SPR [18]. The absorbance peak

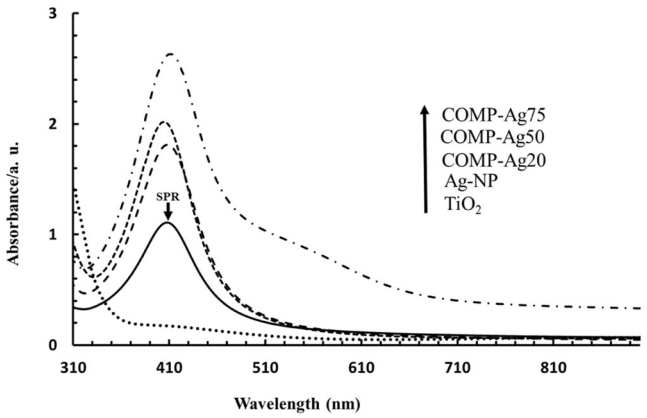

FIGURE 5 UV–Vis absorption spectra for a TiO_2 (dotted line), Ag NP (thick solid line), and COMP-Ag20, 50 and 75 Ag mol% (dashed line) thin films, fabricated on quartz glass.

TABLE 2 The Hall effect measured and calculated on COMP-Agn thin films.

Notation (n)	Resistance (R Ω)[a]	Bulk resistivity ($\rho\Omega$cm)[a] at 300 K	Sheet resistance ($R_s\ \Omega/\blacksquare$)	Electron mobility (μ $cm^2V^{-1}S^{-1}$)	Carrier concentration ($N\ cm^{-3}$)	Carrier type
COMP-Ag20	3918 (314)	0.192 (0.12)	1.28×10^4	1.3×10^1	-1.9×10^{14}	n
COMP-Ag45	10,458 (1446)	74.3 (1.10)	7.43×10^4	1.3×10^1	-1.2×10^{12}	n
COMP-Ag50	6.2 (6.0)	5.8×10^{-4} (4.2×10^{-4})	58.0	3.9×10^3	8.3×10^{14}	p
COMP-Ag60	5.5 (3.2)	1.7×10^{-4} (1.0×10^{-5})	17.0	5.1×10^3	3.0×10^{18}	p
COMP-Ag75	1.5 (1.2)	6.9×10^{-5} (3.0×10^{-5})	6.27	7.80×10^2	1.3×10^{19}	p

[a]The standard deviations are presented in parentheses.

maxima for the COMP-Ag20, COMP-Ag50, and COMP-Ag75 were at 410–413 nm, respectively. COMP–Ag75 exhibits a dramatic rise in absorbance, as well as two unique absorption peaks: one at 415–425 nm, and the other at 550–550 nm. Both SPR and LSPR are responsible for this. With more Ag-NPs in the titania matrix, the SPR peak rises, which improves the TiO_2's photo responsiveness in the visible range [29]. As a result, the plasmonic feature of Ag NPs can make it easier to understand the mechanism underlying the production of cathodic photocurrent from the Ag NP/TiO_2 composite thin films reported in our previous papers [22, 23]. By creating a strong electromagnetic field close to the surface of the metal nanoparticles and increasing the dye's ability to absorb light in the visible range of wavelengths, LSPR can increase the solar conversion efficiency of DSSCs [69]. But prior studies revealed that adding metal nanoparticles to a DSSC reduced its effectiveness because the oxide semiconductors' direct interaction with the dye molecules limited the surface area available for light absorption [70].

FTIR and absorption spectra of the extracted chlorophyll

The infrared spectrum of dye derived from mopane leaves' chlorophyll is displayed in Figure 6. To confirm that the extract is chlorophyll, the obtained spectrum was compared to the library spectrum of chlorophyll. The mid-infrared region (4000, 200 cm^{-1}) is visible in the dye's FTIR spectra as functional groups, with the sharpest peak of C–O appearing at 1033.09 cm^{-1}, the widest peak of O–H appearing at 3339.9 cm^{-1}, and the lowest peak intensity of amines appearing at 1012.6 cm^{-1}. Moreover, distinct functional forms of C–H_3, C–H_2, C═O, C═C, aromatic, and C–N were also visible in the spectra, occurring at 2923.49, 2864, 1734.1, 1615.2, 1452.6, and 1373.3 cm^{-1}, respectively. The outcome in this spectrum is in line with the findings of Al-Alwani and his team [71]. Given that this FTIR spectrum and the chlorophyll library spectrum have similar functional groups, it is secure to infer that the dye extracted and employed in this study is, in fact, chlorophyll.

The UV-Vis absorption spectrum of mopane leaves' derived chlorophyll dye is shown in Figure 7. The extracted dye exhibits two distinct, visible absorption peaks with peak maximums at 425 and 665 nm. This verified that the pigment produced was a mixture of chlorophyll-*a* and -*b* [27, 33, 61, 62]. The extracted chlorophyl-*a* and -*b* had concentrations of 0.53 and 0.42 mg/L, respectively. As anticipated and documented in the literature, chlorophyll-*a* is present in higher concentrations than chlorophyll-*b* [72].

Absorption spectrum of the extracted chlorophyll

The UV-vis absorption spectra of COMP-AgnChl (Ag-NP/TiO_2/chlorophyll dye), and TiO_2-Chl are shown in Figure 8. The TiO_2-Chl had a generally low-intensity absorption band, but its absorption intensity rose sharply at wavelengths between 425 and 700. Due to its overlap with peak maximums at 425 and 665 nm of chlorophyll, this indicates that chlorophyll dye boosted TiO_2 absorption in visible light. Notably, as compared to the absorption in Figure 5, red shifting was observed in all peaks in Figure 8.

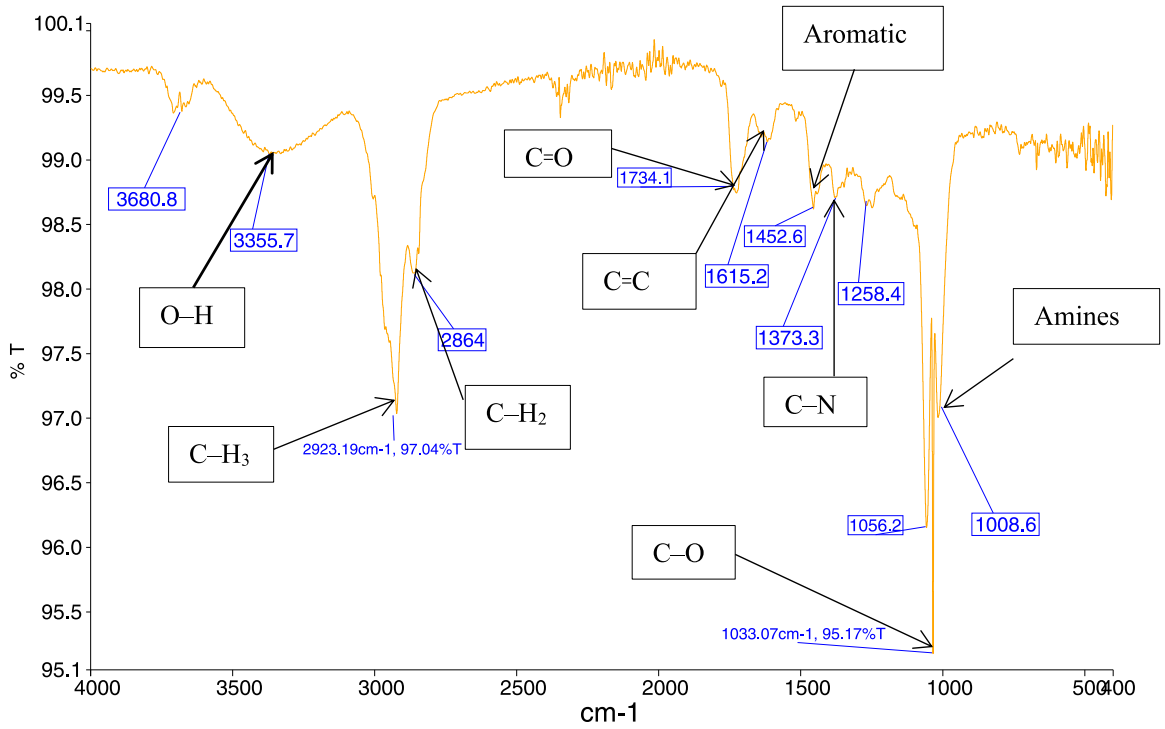

FIGURE 6 Fourier-transform infrared spectroscopy spectrum of the Chlorophyll dye extracted from Mopane leaves.

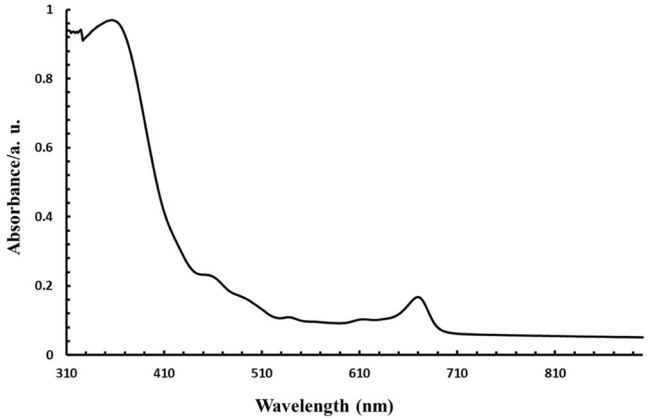

FIGURE 7 UV-vis absorption spectra of Chlorophyll dye sensitizer.

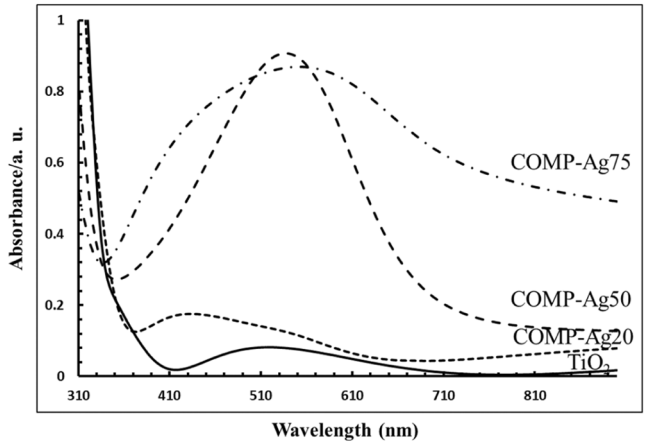

FIGURE 8 UV–Vis absorption spectra for a TiO_2-Chl (thick solid line) and COMP-Agn/Chl with n = 25, 50, and 75 Ag mol% (dashed lines) thin films, fabricated on quartz glass.

When chlorophyll was adsorbed onto the COMP-Ag-n/Chl thin films, they displayed a significant absorbance enhancement, which can be explained by SPR [22] and metal-to-ligand charge transfer (MLCT), [73] via which the photoelectric charge is injected into the TiO_2. Interestingly, red shifting was shown across every one of the peaks in Figure 8 in comparison to the absorption in Figure 5. The absorbance peaks in every COMP-Agn/Chl were boosted toward the longer wavelength of 500 nm. Pure TiO_2 and COMP-25 do not allow more chlorophyll dye to be adsorbed, thereby not improving the absorbance spectra intensities in the long wavelength range. The COMP-Ag50/Chl had a strong, identifiable absorption peak in the 400–650 nm range, with the largest absorbance peak at 540 nm. When compared to the COMP-Ag20/Chl, unquestionably there is an improvement. The thin film of the COMP-Ag75/Chl had a prominent, wider absorbance peak that covered the visible-infrared region. Besides that, the surface plasmonic resonance of Ag-TiO_2 makes COMP-Ag75/Chl a p-type semiconductor that can be utilized in visible light photocatalytic applications [22].

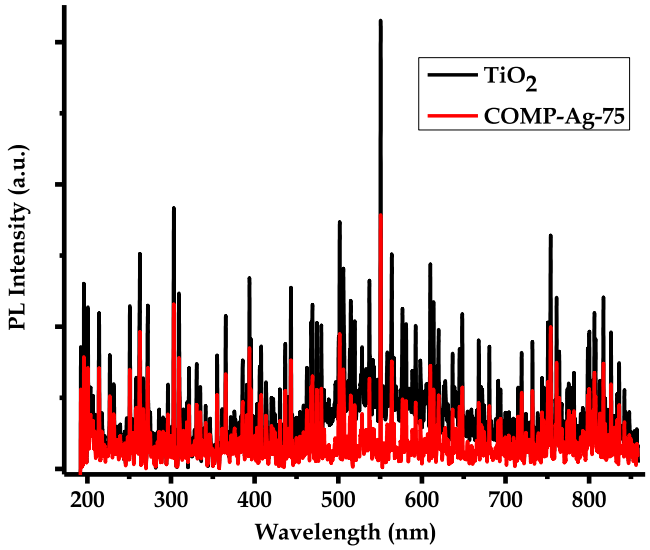

FIGURE 9 Comparison of the photoluminescence spectra of samples TiO_2 and COMP-Ag75.

PL spectra

The PL emission spectra were used to investigate the efficiency of charge carrier trapping, immigration, transfer, and separation, and to understand the fate of photogenerated electrons and holes in the semiconductor since PL emission results from the recombination of free carriers. Figure 9 presents a comparison of the PL spectra of samples TiO_2 and COMP-Ag75 in the wavelength range of 300–800 nm.

PL spectra results confirm that the prepared samples are efficient in photoconversion, immigration of electrons/holes, and photoluminescence processes [74, 75]. For pure TiO_2, there is a wide PL spectrum emission peak between 423 and 650 nm, [74–76] while for other COMP-Ag-75, it has no emission peak. Thus, fluorescence quenching is observed for COMP-Ag-75, indicating that the Ag doping successfully prevented the unnecessary e−/h+ pair recombination, leading to reduction of recombination rate, in consistency with other work [75, 76]. The decrease of recombination rate should enhance the charge carrier separation, resulting in more free charges that can contribute to the PCE process.

PCE of the assembled p-DSSC

Figure 10 shows the current–voltage (IV) curve for p-DSSC with Ag/TiO_2 photoanode consisting of 75% Ag in TiO_2 matrix of Ag coated with chlorophyll dye. The IV-curve demonstrates that the cell functions when illuminated (by light). The IV-curve displays a zero current when there is no light. This suggests that when there is no light present, the cell does not generate any current. By dividing area A by area B, the FF and the efficiency of the cell was calculated. Table 3 lists the PV property values of silver-nanoparticles/titania p-type dye sensitized solar cell and compared to PV properties values

obtained from by other studies for p-type DSSCs and for the Ag doped TiO_2-based DSSCs.

From Table 3, the p-DSSC device under our investigation has the efficiency of 0.37%, the J_{sc} is 0.022 mA cm^2, V_{oc} is 174 mV and FF is 0.335. This implies that the prepared Ag/TiO_2 with 75 mol% of Ag can be used as a working electrode for DSSC since it has enough energy level for hole extraction [74]. However, as it can be seen from Table 3 that the p-type DSSCs have a much lower PCE compared to the n-types. The FF generated is almost like those of other p-type DSSCs as presented in Table 3. All their *FF* are still lower, compared to those of n-type DSSCs, which can be attributed to the relatively low shunt resistance (R_s) from the thin films [83].

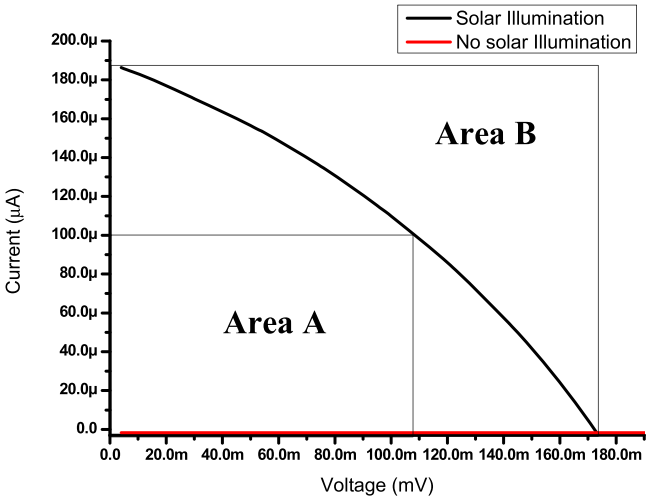

FIGURE 10 IV curve for the assembled COMP-Ag75/Chl-activated carbon/fluorine-doped tin oxide dye-sensitized solar cells, used for fill factor and photon-electrical conversion efficiency (PCE) calculation.

As shown in Table 3, the J_{sc} and V_{oc} both show significant regular variation with corresponding Ag–NP additions to TiO_2. It is evident that the J_{sc} and V_{oc} both increased with the quantity of Ag–NP ranging from 0 to 2.5 wt%. However, they began to decrease when the Ag–NPs content was more than 0.25 wt%. The increase in J_{sc} is attributable to the enhanced dye light absorption in intensity and spectral range caused by the SPR of Ag–NPs in the photoanode, whereas the increase in V_{oc} may be attributable to the more negative level of the quasi-Fermi energy of the Ag–TiO_2 composite system caused by the addition of Ag [82]. However, the J_{sc} and V_{oc} both decreased when the Ag–NPs content reached 0.20 wt%. The reason for this may be explained as follows: Not all the Ag–NPs in Ag@TiO_2 were entirely incorporated into TiO_2 matrix. Therefore, some of the bare Ag–NPs in the Ag–TiO_2 network structure may be eroded by electrolyte and oxidized to Ag+ ions [23]. The oxidation of the Ag will act as new recombination center, thus reducing the number of the charge carrier led to decrease in the J_{sc} and V_{oc}. Consequently, the overall conversion efficiency of the DSSC would have deteriorated. In addition, Ag–NPs (over 2.5 wt%) incorporated into the TiO_2 films

TABLE 3 Values of V_{oc}, I_{sc}, J_{sc}, *FF*, and photovoltaic conversion efficiency of dye-sensitized solar cells as a function of A-NP loading in TiO_2 obtained from Figure 9 and from literatures.

Assembled p-DSSC (sandwich)	Counter electrode type	V_{oc} (mV)	Isc (μA)	J_{sc} (mA/cm^2)	FF (ratio)	η %	Reference
COMP-Ag75/Chl-AC/FTO	p	174	187	0.022	0.335	0.37	This study
NiO-Cobalt Redox Couples	p	275	-	2.65	0.330	0.24	[35]
NiO	p	55.0	-	1.36	0.340	0.03	[77]
K-doped ZnO	p	82.0	-	0.408	0.350	0.012	[9]
$CuFeO_2$	p	365		0.071	0.390	0.010	[78]
20.0 wt%Ag@TiO_2	n	750	-	9.96	0.480	3.59	[79]
10.0 wt@Ag@TiO_2	n	770	-	9.93	0.490	3.75	[79]
2.5 wt%Ag@TiO_2	n	490	-	2.099	0.409	0.421	[80]
2.5 wt%Ag@TiO_2	n	770	-	12.19	0.520	4.89	[79]
2.0 Wt% Ag@TiO_2	n	686	-	10.19	0.660	4.10	[81]
2.0 Wt% Ag@TiO_2	n	644	-	10.09	0.467	3.01	[82]
1 wt% Ag@TiO_2	n	770	-	8.17	0.630	3.89	[79]
0.20 wt%Ag@TiO_2	n	686	-	8.23	0.66	4.10	[81]
0.15 wt%Ag@TiO_2	n	698	-	10.19	0.67	5.33	[81]
TiO_2	n	710	-	6.71	0.540	2.57	[79]

Note: V_{oc}: Open-circuit voltage; I_{sc}: Short circuit current; J_{sc}: Short circuit current density.
Abbreviations: FF, fill factor; η, photovoltaic conversion efficiency (PCE).

might result in a reduced effective surface area of TiO_2 in contact with dye molecules. Consequently, the recombination probability between electrons and holes may increase, so J_{sc} would decrease. In addition, higher concentrations of Ag–NPs may cluster to form larger Ag–NP groups with lower electron storage capability, reducing V_{oc} [22]. It is reported that, the surface plasmonic resonance of Ag/TiO_2 with wt% greater than 45 makes $Ag\text{-}TiO_2$ based composite a p-type semiconductor [21].

Incorporation of silver nanoparticles into the matrix of titania results in a decrease of electrical resistivity. Metallic silver nanoparticles add charge carriers to titania, improving bulk conductivity [22, 23]. At the same time, the surface plasmonic resonance of Ag/TiO_2 m at mol% greater than 45 makes $Ag\text{-}TiO_2$-based composite a p-type semiconductor [21]. TiO_2 doped Ag has the capacity to absorb visible light, making it a viable resource for converting solar energy. The ability of SPR to increase light scattering in thin films, improve near fields by applying an electric field, and directly generate charge carriers in semiconductors has been reported to have improved PV device efficiencies [15–17, 20, 23, 56, 69, 81]. However, as shown in the SEM image for the same electrode we are reporting here, [22, 23] free-standing Ag nanoparticles may be oxidized to Ag(I) [81] and degraded by the electrolyte, [84] which could explain why a lower PCE is observed in our DSSC. As Ag oxidizes, it becomes more reactive, creating a new recombination site. Consequently, fewer charge carriers will result in fewer electron-hole recombination, and thus J_{SC} value is lower. This also may result in lower p-DSSC conversion efficiency. As we can see, all p-type DSSCs generate a very low J_{sc} values compared to n-type DSSCs. Each component of a DSSC affects how well the solar cell works. A good DSSC is made by finding the best balance between the components. The choice of photoelectrode material and its structure determines the current–voltage characteristics, that is, V_{oc}, J_{sc}, light scattering/absorption properties, dye pickup, and the cell's *FF* [85].

Proposed mechanism for PV properties of plasmonic Ag NP/TiO_2 photocathode working electrode-based DSSC

Although it has been reported [22, 23] that the inclusion of Ag in the Titania matrix thin film fabricated vis MPM has no effect on the band gap of TiO_2. The presence of wavelength shift at the TiO_2 thin film absorption edges in the spectra of the Ag NP/TiO_2 in the presence of Chlorophyll dye shows that the band gap of TiO_2 was altered by the inclusion of chlorophyll. Additionally, the UV-Vis absorption spectra demonstrated that the Ag NPs' well-defined SPR peaks and broad-range LSPR bands may effectively sensitize the Ag/TiO_2 thin films. As a result, these SPR and LSPR characteristics of the Ag NP/TiO_2 thin films can aid in our understanding of the mechanism underlying p-DSSC PV generation. Hence, the charge transfer processes that occur in a p-DSSC under operation are summarized as follows and illustrated by seven steps in Figure 11 [4, 25, 86–88].

These are listed below:

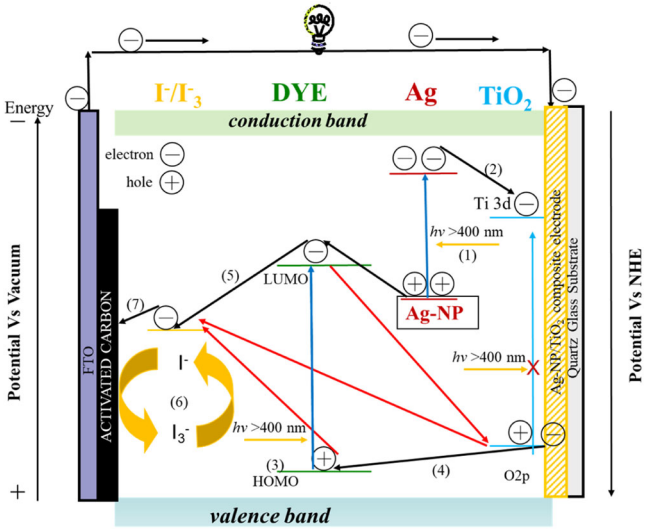

FIGURE 11 The electronic mechanism taking place in a p-dye-sensitized solar cells: The black lines show the mobility of the electrons (and holes) in a COMP-Ag75 based p-DSSC, while the blue lines show light-induced photoexcitation. Unwanted recombination reactions are represented by red lines.

(1) Ag NPs electrons in TiO_2 Matrix gain access to higher band states because of LSPR.
(2) If they have enough energy, these electrons move into the TiO_2 conduction band (CB) [23].
(3) Simultaneously, the chlorophyll dye is stimulated by light to form an electronic excited state (D*):

$$D + hv \rightarrow D^*.$$

(4) Electron transfer from the p-type Ag/TiO_2's valence band (VB) takes place to reduce the dye:

$$D^* + Ag\ /TiO_2 \rightarrow D - +Ag\ /TiO_2|h^+.$$

(5) The photoexcited electrons then enter the electrolyte more quickly.
(6) In three steps, radical-containing oxidized species in the electrolyte regenerate the ground state of the dye.

$$D - +I^{3-} \rightarrow D + I^{2\cdot-} + I^- \text{ Step 1.}$$

Triiodide initially regenerates the reduced dye to create the diiodide radical [25, 86]. This disproportionate to create iodide and triiodide.

$$2I^{2\cdot-} \rightarrow I^{3-} + I^- \text{ Step 2.}$$

Regeneration of the reduced species in the iodide/triiodide occurs at the CE:

$$3I^- \rightarrow I3^- + 2e^- \text{ Step 3.}$$

(7) The CE produces a cathodic PV. The cycle is then completed when the electrons join this same device now at working electrode after passing through the external circuit.

The following recombination routes (highlighted in red in Scheme 2) compete with these steps forward charge transfer processes in three ways:

(i) Dye degradation in the excited state (radiative and nonradiative):

$$D^* \rightarrow D + hv.$$

(ii) Recombination of charge among a reduced dye and a hole in p-type Ag/TiO_2:

$$D - + Ag\ /TiO_2|h + \rightarrow D + Ag\ /TiO_2.$$

(iii) Recombination of a hole's charge with the reduced species in the electrolyte:

$$2[Ag\ /TiO_2|h^+] + 3I^- \rightarrow NiO + I^{3-}.$$

The opposite of cathodic PV is experienced in n-DSSC. An anodic PV can be created if the potential coming from the CE is high enough to force electrons to flow to the conductive substrate from the CB of TiO_2 rather than into the electrolyte, depending on the redox potential difference between the composite thin film and CE [4, 25, 87, 88]. The simple explanation provided by Figure 9 here explains why the metal oxide thin films exhibit a cathodic PV, even if the general inferences that can be made from this proposed mechanism are perfectly consistent with the results reported earlier [15, 18, 19, 22, 42]. At this time, the literature does not explain for the plasmonic conductive p-type Ag/TiO_2 based DSSC [4, 25, 87, 88].

CONCLUSIONS

In this study, we demonstrated for the first time that an Ag/TiO_2 composite thin film fabricated via MPM may function as a photocathode electrode in a DSSC with up to charge carrier concentrations of $1.3 \times 10^{-19}\ cm^{-3}$. When the amount of Ag nanoparticles in the TiO_2 matrix was increased, the plasmon peak at 410 nm was visible and the electrical conductivity of the composite thin films improved to 6.7×10^{-5} cm, eliminating the need for additional TCO electrodes and enhancing the working electrode's light responsiveness. The photo-response threshold of the Ag-NP/TiO_2 thin films was improved and shifted into the visible and near infrared when the chlorophyll dye was adsorbed onto them. An Ag/TiO_2 based p-DSSC was then developed with coordinated materials development efforts to realize its full potential. This p-DSSC exhibits the PCE of (0.37) %. The J_{sc} is (0.022) mA cm^2, V_{oc} is (174) mV and FF is (33.5) %. This implies that the prepared Ag/TiO_2 with 75 mol% of Ag can be used as an electrode for DSSC since it has sufficient energy level for hole extraction. Just like other p-DSSCs, this p-type DSSC perform very badly. With the potential to create tandem (p-n DSSCs) with efficiencies that are equal to or greater than those of traditional high-efficiency n-DSSCs, this breakthrough will however open the door to produce a new generation of highly efficient photocathodic p-DSSCs. We can advise pairing the TiO_2-based photoanode with a Ag/TiO_2 photocathode in a tandem device to enhance the performance of DSSCs. The V_{OC}, which is low in this paper, is most likely to be equal to the sum of the individual values of the two devices, n-type (TiO_2) and p-type (Ag/TiO_2). Improvement of this solar cell can be done by considering also the novel iodide-free redox mediators, such as $[Co(en)_3]^{2+/3+}$ and $[Fe(acac)_3]^{0/1-}$ based electrolytes, to be explored and may greatly improve device efficiency by producing photosensitizers that promote charge separation. As a result, more light can be successfully captured.

ACKNOWLEDGMENTS

The authors are grateful to the UNAM for providing support and facility to conduct this research and the Centre of Research Service (CRS) for providing technical help and support. This research received external funding from National Commission Research Science and Technology (NCRST), under the call to strengthen research capacity at universities and research institutions (April 2017 to March 2020). Research project titled “Renewable Energy Initiative Project.”

CONFLICT OF INTEREST STATEMENT

The authors declare no conflict of interest.

DATA AVAILABILITY STATEMENT

The data that support the findings of this study are openly available in University of Namiba Library Thesis and dissertation collection at https://unam.on.worldcat.org/search?queryString=kalipi+loini&submit2=Search.

ORCID

Likius S. Daniel https://orcid.org/0000-0003-1221-1852

REFERENCES

[1] B. O'Regan, M. Grätzel, *Nature* **1991**, *353*(6346), 737.
[2] M. Bonomo, S. Sheehan, D. P. Dowling, L. Gontrani, D. Dini, *ChemistrySelect* **2018**, *3*(24), 6729.
[3] M. Bonomo, E. J. Ekoi, A. G. Marrani, A. Y. S. Zarate, D. P. Dowling, C. Barolo, D. Dini, *Energy Fuels* **2021**, *5*(18), 4736.
[4] A. Nattestad, A. J. Mozer, M. K. R. Fischer, Y. B. Cheng, A. Mishra, P. Bäuerle, U. Bach, *Nat. Mater.* **2010**, *9*(1), 31.
[5] R. Jose, V. Thavasi, S. Ramakrishna, *J. Am. Ceram. Soc.* **2009**, *92*(2), 289.
[6] P. Semalti, S. N. Sharma, *J. Nanosci. Nanotechnol.* **2020**, *20*(6), 3647.
[7] A. Morandeira, G. Boschloo, A. Hagfeldt, L. Hammarström, *J. Phys. Chem. B* **2005**, *109*(41), 19403.
[8] J. He, H. Lindström, A. Hagfeldt, S. E. Lindquist, *J. Phys. Chem. B* **1999**, *103*(42), 8940.
[9] J. Bai, X. Xu, L. Xu, J. Cui, D. Huang, W. Chen, Y. Cheng, Y. Shen, M. Wang, *ChemSusChem* **2013**, *6*(4), 622.
[10] A. Wuttig, J. W. Krizan, J. Gu, J. J. Frick, R. J. Cava, A. B. Bocarsly, *J. Mater. Chem. A* **2017**, *5*(1), 165.
[11] X. Xu, J. Cui, J. Han, J. Zhang, Y. Zhang, L. Luan, G. Alemu, Z. Wang, Y. Shen, D. Xiong, W. Chen, Z. Wei, S. Yang, B. Hu, Y. Cheng, M. Wang, *Sci. Rep.* **2014**, *4*(1), 3961.
[12] I. Papadopoulos, P. R. Schol, J. Garcés-Garcés, Á. Sastre-Santos, F. Fernández-Lázaro, D. M. Guldi, *Sol. Energy* **2023**, *250*, 1.

[13] N. A. Narewadikar, K. Y. Rajpure, *Nanobiotechnol. Rep*. **2022**, *17*(1), 39.
[14] P. Akhter, A. Arshad, A. Saleem, M. Hussain, *Catalysts* **2022**, *12*(11), 1331.
[15] C. Vanlalhmingmawia, S. M. Lee, D. Tiwari, *J. Water Process Eng*. **2023**, *51*, 103360.
[16] H. K. Jun, M. A. Careem, A. K. Arof, *Mater. Today Proc*. **2016**, *3*, S73.
[17] S. Shah, I. M. Noor, J. Pitawala, I. Albinson, T. M. W. J. Bandara, B. E. Mellander, A. K. Arof, *Opt. Mater. Express* **2017**, *7*(6), 2069.
[18] S. Shah, Z. H. Z. Abidin, I. M. Noor, Z. Osman, A. K. Arof, *Mol. Cryst. Liq. Cryst*. **2023**, 1. Ahead of Print.
[19] N. C. Jeong, C. Prasittichai, J. T. Hupp, *Langmuir* **2011**, *27*(23), 14609.
[20] Z. Bao, N. Fu, Y. Qin, J. Lv, Y. Wang, J. He, Y. Hou, C. Jiao, D. Chen, Y. Wu, J. Dai, *ACS Appl. Mater. Interfaces* **2020**, *12*(1), 538.
[21] D. S. Likius, H. Nagai, S. Aoyama, C. Mochizuki, H. Hara, N. Baba, M. Sato, *J. Mater. Sci*. **2012**, *47*, 389022.
[22] L. Daniel, H. Nagai, N. Yoshida, M. Sato, *Catalysts* **2013**, *3*(3), 625.
[23] L. S. Daniel, H. Nagai, M. Sato, *J. Mater. Sci*. **2013**, *48*, 7162.
[24] M. K. Nazeeruddin, A. Kay, I. Rodicio, R. Humphry-Baker, E. Müller, P. Liska, M. Grätzel, *J. Am. Chem. Soc*. **1993**, *115*(14), 6382.
[25] E. Benazzi, J. Mallows, G. H. Summers, F. A. Black, E. A. Gibson, *J. Mater. Chem. C* **2019**, *7*(34), 10409.
[26] M. Alhamed, A. S. Issa, A. W. Doubal, *JED* **2012**, *16*, 1370.
[27] R. Baby, P. D. Nixon, N. M. Kumar, M. S. P. Subathra, N. Ananthi, *Environ. Sci. Pollut. Res*. **2021**, *29*, 371.
[28] M. S. Abdel-Latif, M. B. Abuiriban, T. M. El-Agez, S. A. Taya, *Int. J. Renew. Energy Res*. **2015**, *5*, 294.
[29] C. Cari, A. Khairuddin, T. Y. Septiawan, P. M. Suciatmoko, D. Kurniawan, A. Supriyanto, *AIP Conf. Proc*. **2018**, *2014*, 020106. https://doi.org/10.1063/1.5054510
[30] A. Torchani, S. Saadaoui, R. Gharbi, M. Fathallah, *Curr. Appl. Phys*. **2015**, *15*, 307.
[31] A. Lim, N. Haji Manaf, K. Tennakoon, R. L. N. Chandrakanthi, L. B. L. Lim, J. M. R. S. Bandara, P. Ekanayake, *J. Biophys*. **2015**, *2015*, 1. https://doi.org/10.1155/2015/510467
[32] D. Ganta, J. Jara, R. Villanueva, *Chem. Phys. Lett*. **2017**, *679*, 97.
[33] A. Sen, M. H. Putra, A. K. Biswas, A. K. Behera, A. Groβ, *Dyes Pigm*. **2023**, *213*, 111087.
[34] L. Giribabu, R. Bolligarla, M. Panigrahi, *Chem. Record* **2015**, *15*(4), 760.
[35] E. A. Gibson, A. L. Smeigh, L. Le Pleux, L. Hammarström, F. Odobel, G. Boschloo, A. Hagfeldt, *J. Phys. Chem. C* **2011**, *115*(19), 9772.
[36] I. R. Perera, T. Daeneke, S. Makuta, Z. Yu, Y. Tachibana, A. Mishra, P. Bäuerle, C. A. Ohlin, U. Bach, L. Spiccia, *Angew. Chem. Int. Ed*. **2015**, *54*(12), 3758.
[37] M. Wang, A. M. Anghel, B. Marsan, N. L. Cevey Ha, N. Pootrakulchote, S. M. Zakeeruddin, M. Grätzel, *J. Am. Chem. Soc*. **2009**, *131*, 15976.
[38] S. Powar, Q. Wu, M. Weidelener, A. Nattestad, Z. Hu, A. Mishra, U. Bach, *Energy Environ. Sci*. **2012**, *5*(10), 8896.
[39] S. Mathew, A. Yella, P. Gao, R. Humphry-Baker, B. F. E. Curchod, N. Ashari-Astani, I. Tavernelli, U. Rothlisberger, M. K. Nazeeruddin, M. Grätzel, *Nat. Chem*. **2014**, *6*(3), 242.
[40] X. L. Zhang, Z. Zhang, D. Chen, P. Bäuerle, U. Bach, Y. B. Cheng, *Chem. Commun*. **2012**, *48*(79), 9885.
[41] A. Zaban, M. Greenshtein, J. Bisquert, *Chemphyschem* **2003**, *4*(8), 859.
[42] W. J. Lee, E. Ramasamy, D. Y. Lee, J. S. Song, *ACS Appl. Mater. Interfaces* **2009**, *1*(6), 1145.
[43] S. Imani, A. Alizadeh, M. Roudgar-Amoli, Z. Shariatinia, *Inorg. Chem. Commun*. **2022**, *145*, 110045.
[44] J. Gong, K. Sumathy, Q. Qiao, Z. Zhou, *Renew. Sustain. Energy Rev*. **2017**, *68*, 234.
[45] E. Akman, H. S. Karapinar, *Sol. Energy* **2022**, *234*, 368.
[46] A. A. Arbab, K. C. Sun, I. A. Sahito, M. B. Qadir, Y. S. Choi, S. H. Jeong, *ACS Appl. Mater. Interfaces* **2016**, *8*, 7471.
[47] K. S. G. C. Oliveira, K. M. Barcelos, J. J. Lado, J. Palma, L. A. M. Ruotolo, *Chem. Eng. J*. **2023**, *457*, 141059.
[48] P. Bröms, J. Birgersson, N. Johansson, M. Lögdlund, W. R. Salaneck, *Synth. Met*. **1995**, *74*(2), 179.
[49] A. Andersson, N. Johansson, P. Bröms, N. Yu, D. Lupo, W. R. Salaneck, *Adv. Mater*. **1998**, *10*(11), 859.
[50] A. Way, J. Luke, A. D. Evans, Z. Li, J. S. Kim, J. R. Durrant, H. K. Hin Lee, W. C. Tsoi, *AIP Adv*. **2019**, *9*(8), 085220.
[51] G. Kiruthiga, K. S. Rajni, T. Raguram, N. Eswaramoorthy, S. Pitchaiya, In *IOP Conference Series: Materials Science and Engineering*, 1263(No. 1), IOP Publishing, **2022**, 012020. https://doi.org/10.1088/1757-899X/1263/1/012020
[52] J. Navarro-Arenas, J. Parra, P. Sanchis, *IEEE J. Quantum Electron*. **2023**, *59*, 1.
[53] Z. Ning, Y. Fu, H. Tian, *Energy Environ. Sci*. **2010**, *3*(9), 1170.
[54] A. Renaud, B. Chavillon, L. Le Pleux, Y. Pellegrin, E. Blart, M. Boujtita, T. Pauporté, L. Cario, S. Jobic, F. Odobel, *J. Mater. Chem*. **2012**, *22*(29), 14353.
[55] N. H. Shamsudin, S. Shafie, M. Z. A. Ab Kadir, F. Ahmad, Y. Sulaiman, S. A. M. Chachuli, M. C. Razali, *Optik* **2023**, *272*, 170237.
[56] M. Chinnarani, K. M. Prabu, S. Suresh, *Results Chem*. **2023**, *5*, 100835.
[57] N. Kumar, S. Lenita, G. K. Parvathi, I. R. Rupa, M. Shafreen, M. Danish, In *Nanocomposites-Advanced Materials for Energy and Environmental Aspects*, Woodhead Publishing, **2023**, pp. 225. https://doi.org/10.1016/B978-0-323-99704-1.00004-7
[58] H. Nagai, M. Sato, *Advanced Coating Materials*, Scrivener Publishing LLC, **2018**, ch.1.
[59] M. Sato, H. Hara, T. Nishide, Y. Sawada, *J. Mater. Chem*. **1996**, *6*(11), 1767.
[60] H. Nagai, S. Aoyama, H. Hara, C. Mochizuki, I. Takano, N. Baba, M. Sato, *J. Mater. Sci*. **2009**, *44*, 861.
[61] M. A. M. Al-Alwani, N. A. Ludin, A. B. Mohamad, A. A. H. Kadhum, K. Sopian, *Spectrochim. Acta, Part A* **2017**, *179*, 23.
[62] H. Zhou, L. Wu, Y. Gao, T. Ma, *J. Photochem. Photobiol., A* **2011**, *219*(2-3), 188.
[63] H. K. Lichtenthaler, C. Buschmann, *Curr. Protoc. Food Anal. Chem*. **2001**, *1*(1), F4.
[64] F. Johan, M. Z. Jafri, H. S. Lim, W. W. Maznah, In *2014 IEEE International Conference on Industrial Engineering and Engineering Management*, IEEE, Selangor, Malaysia, **2014**, 744. https://doi.org/10.1109/IEEM.2014.7058737
[65] A. Rahman, H. J. Hango, L. S. Daniel, V. Uahengo, S. J. Jaime, S. V. H. S. Bhaskaruni, S. B. Jonnalagadda, *J. Clean. Prod*. **2019**, *237*, 117689.
[66] L. Luo, Y. Lan, Q. Zhang, J. Deng, L. Luo, Q. Zeng, H. Gao, W. Zhao, *J. Energy Storage* **2022**, *55*, 105839.
[67] L. R. V. Buizza, A. D. Wright, G. Longo, H. C. Sansom, C. Q. Xia, M. J. Rosseinsky, M. B. Johnston, H. J. Snaith, L. M. Herz, *ACS Energy Lett*. **2021**, *6*(5), 1729.
[68] T. T. Loan, V. H. Huong, V. T. Tham, N. N. Long, *Phys. B Condens. Matter* **2018**, *532*, 210.
[69] W. Hou, Z. Liu, P. Pavaskar, W. H. Hung, S. B. Cronin, *J. Catal*. **2011**, *277*(2), 149.
[70] C. K. N. Peh, L. Ke, G. W. Ho, *Mater. Lett*. **2010**, *64*(12), 1372.
[71] R. Syafinar, N. Gomesh, M. Irwanto, M. Fareq, Y. M. Irwan, *Energy Proc*. **2015**, *79*, 896.
[72] H. Irie, S. Miura, K. Kamiya, K. Hashimoto, *Chem. Phys. Lett*. **2008**, *457*(1-3), 202.

[73] U. Veikko, X. Zhang, T. Peng, P. Cai, G. Cheng, *Spectrochim. Acta Part A* **2013**, *105*, 539.
[74] H. S. Mohamed, M. Rabia, X. G. Zhou, X. S. Qin, G. Khabiri, M. Shaban..., B. L. Su, *J. Mater. Sci. Technol*. **2021**, *83*, 179.
[75] Z. D. Mahmoudabadi, E. Eslami, M. Narimisa, *J. Colloid Interface Sci*. **2018**, *529*, 538.
[76] F. Wang, Z. Lu, H. Guo, G. Zhang, Y. Li, Y. Hu, W. Jiang, G. Liu, *Chem. A Eur. J*. **2023**, *29*, e202202716.
[77] P. Qin, J. Wiberg, E. A. Gibson, M. Linder, L. Li, T. Brinck, A. Hagfeldt, B. Albinsson, L. Sun, *J. Phys. Chem. C* **2010**, *114*(10), 4738.
[78] T. Zhu, Z. Deng, X. Fang, Z. Huo, S. Wang, W. Dong, J. Shao, R. Tao, C. Song, L. Wang, *J. Alloys Compd*. **2016**, *685*, 836.
[79] S. P. Lim, A. Pandikumar, N. M. Huang, H. N. Lim, *RSC Adv*. **2014**, *4*(72), 38111.
[80] R. G. Nair, S. Ojah, P. M. Kumar, S. K. Nikhil, S. K. Samdarshi, *Mater. Lett*. **2018**, *221*, 313.
[81] K. Guo, M. Li, X. Fang, X. Liu, B. Sebo, Y. Zhu, Z. Hu, X. Zhao, *J. Power Sources* **2013**, *230*, 155.
[82] V. Rajakani, X. S. Shajan, A. Arulgnanam, P. S. Premkumar, *Mater. Today Proc*. **2022**, *65*, 2473.
[83] J. H. Park, J. Seo, S. Park, S. S. Shin, Y. C. Kim, N. J. Jeon, H. W. Shin, T. K. Ahn, J. H. Noh, S. C. Yoon, C. S. Hwang, S. I. Seok, *Adv. Mater*. **2015**, *27*(27), 4013.
[84] I. Ibrahim, H. N. Lim, N. W. K. Wan, N. M. Huang, S. P. Lim, W. Busayaporn, H. Nakajima, *Sol. Energy* **2021**, *215*, 403.
[85] M. Shakeel Ahmad, A. K. Pandey, N. Abd Rahim, *Renew. Sustain. Energy Rev*. **2017**, *77*, 89.
[86] E. A. Gibson, L. Le Pleux, J. Fortage, Y. Pellegrin, E. Blart, F. Odobel, A. Hagfeldt, G. Boschloo, *Langmuir* **2012**, *28*(15), 6485.
[87] M. Dhonde, K. Sahu, M. Das, A. Yadav, P. Ghosh, V. V. S. Murty, *J. Electrochem. Soc*. **2022**, *169*, 066507.
[88] F. Odobel, L. Le Pleux, Y. Pellegrin, E. Blart, *Acc. Chem. Res*. **2010**, *43*(8), 1063.

How to cite this article: L. S. Daniel, R. T. Kaffer, L. M. Kalipi, A. Rahman, M. Kalengay, V. Uahengo, *Appl. Res*. **2023**, e202300044. https://doi.org/10.1002/appl.202300044